

Molecular docking and 3D-QSAR studies on triazolinone and pyridazinone, non-nucleoside inhibitor of HIV-1 reverse transcriptase

Sree Kanth Sivan · Vijjulatha Manga

Received: 3 September 2009 / Accepted: 6 November 2009 / Published online: 15 December 2009
© Springer-Verlag 2009

Abstract Nonnucleoside reverse transcriptase inhibitors (NNRTIs) are allosteric inhibitors of the HIV-1 reverse transcriptase. Recently a series of Triazolinone and Pyridazinone were reported as potent inhibitors of HIV-1 wild type reverse transcriptase. In the present study, docking and 3D quantitative structure activity relationship (3D QSAR) studies involving comparative molecular field analysis (CoMFA) and comparative molecular similarity indices analysis (CoMSIA) were performed on 31 molecules. Ligands were built and minimized using Tripos force field and applying Gasteiger-Hückel charges. These ligands were docked into protein active site using GLIDE 4.0. The docked poses were analyzed; the best docked poses were selected and aligned. CoMFA and CoMSIA fields were calculated using SYBYL6.9. The molecules were divided into training set and test set, a PLS analysis was performed and QSAR models were generated. The model showed good statistical reliability which is evident from the r_{nv}^2 , q_{100}^2 and r_{pred}^2 values. The CoMFA model provides the most significant correlation of steric and electrostatic fields with biological activities. The CoMSIA model provides a correlation of steric, electrostatic, acceptor and hydrophobic fields with biological activities. The information rendered by 3D QSAR model initiated us to optimize the lead and design new potential inhibitors.

Keywords CoMFA (Comparative molecular field analysis) · CoMSIA (Comparative molecular similarity indices analysis) · Docking · HIV-1 reverse transcriptase · Non-nucleoside inhibitors · Pyridazinones · Triazolinones

Introduction

Human immunodeficiency virus type1 (HIV-1) is responsible for human acquired immunodeficiency syndrome (AIDS), one of the most urgent world health threats. The number of people infected with AIDS has increased to an unprecedented level of 39.5 million [1] throughout the world. HIV-1 genome encodes for three major enzymes protease, reverse transcriptase and integrase for HIV-1 replication. HIV-1 reverse transcriptase (HIV-1 RT), which is virally encoded, is essential for the replication of HIV-1; it converts the viral RNA genome into a double-stranded linear DNA intermediate that is subsequently integrated into the host cell DNA. HIV-1 RT consists of a polymerase domain and RNase H Domain. Two types of drugs that inhibit HIV-1 polymerase activity are nucleoside and nonnucleoside inhibitors. Non-nucleoside reverse transcriptase inhibitors (NNRTIs) are important components of the first line highly active antiretroviral therapy (HAART) regimens. NNRTIs are alleosteric inhibitors; they bind to an induced hydrophobic pocket adjacent to the polymerase active site of HIV-1 RT and prevent the progression of DNA synthesis from the viral RNA template [2]. Binding of NNRTIs to HIV-1 reverse transcriptase is thought to restrict the motion of key residues in the polymerase active site and prevent incorporation of nucleotides into the DNA chain during reverse transcription [3]. The hydrophobic pocket is formed by the key residues like Tyr181, Tyr183, Tyr188 and Thr229. All NNRTIs form direct or water

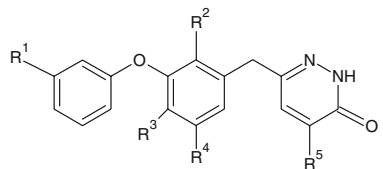
S. K. Sivan · V. Manga (✉)
Department of Chemistry, Nizam college, (O.U),
Basheerbagh, Hyderabad 500 001, India
e-mail: vijjulathamanga@gmail.com

S. K. Sivan
e-mail: sivan.sreekanth@gmail.com

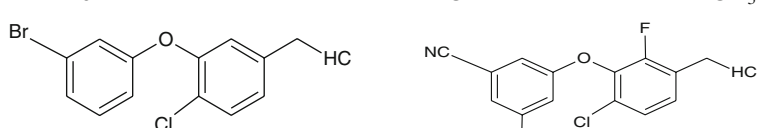
mediated hydrogen bonds with the protein backbone of lysine residue Lys101 or Lys103 [4]. Recently a new series of pyridazinones and triazolinones were reported as potent non-nucleoside reverse transcriptase inhibitors by Sweeney et al. [5–7]. These inhibitors showed hydrogen bond interaction with Lys103 and a good hydrophobic interaction with Tyr181, Tyr188 and Thr229.

Several computational approaches are employed in development and optimization of inhibitors, in present article we report receptor based 3D-QSAR studies using CoMFA [8, 9] and CoMSIA [10] methodologies on pyridazinones and triazolinones derivatives. Partial least square (PLS) [11] based statistical analysis was carried out on 31 molecules to identify the correlation. The contour

Table 1 Structures of compounds



Compound	R ¹	R ²	R ³	R ⁴	R ⁵
1	Cl	H	H	H	H
2	Cl	H	H	-CH ₃	H
3	Cl	H	-CH ₃	H	H
4	Cl	H	Cl	H	H
5	H	H	Cl	H	H
6	H	H	Cl	H	-CH ₃
7	H	F	Cl	H	H
8	H	F	Cl	H	-CH ₃
9	Br	H	Cl	H	-N(CH ₃) ₂
10	Br	H	Cl	H	-CH ₃



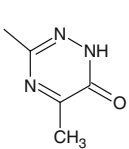
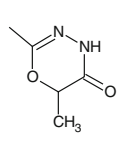
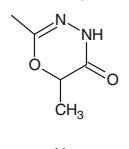
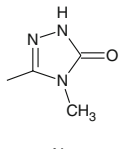
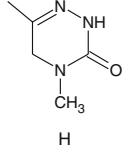
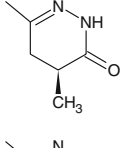
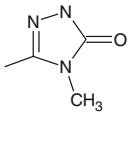
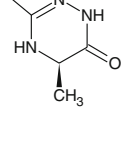
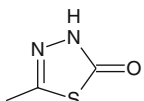
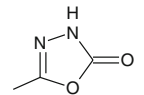
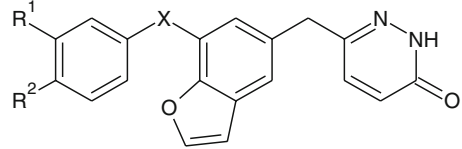
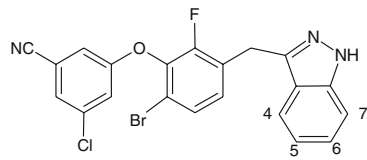
Compound	HC	Compound	HC
11		17	
12		18	
13		19	
14		20	

Table 1 (continued)

15				
16				
				
Compound	R ¹	R ²	X	
21	H	Cl	-C=O	
22	Cl	H	-C=O	
23	Cl	H	-CH ₂	
24	Cl	H	O	
				
Compound	4	5	6	7
25	CH	CH	CH	CCN
26	CH	CH	CH	CNH ₂
27	CH	CH	NCH ₃	C=O
28	CH	CH	CH	N
29	CH	CH	N	CH
30	CH	CH	N	N
31	N	CH	CH	N

maps generated enabled us to explain the observed variation in activity and guided us to design new molecules.

Methodology

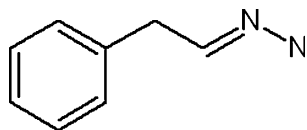
A total of 31 molecules were available with reported IC₅₀ values for inhibition of HIV-1 RT [5–7], these values were converted to corresponding pIC₅₀ values (Table 1). The data set was divided into training set consisting of 24 molecules and test of seven molecules.

All molecular modeling calculations were performed on a Linux operating system. Three dimensional structure building and all modeling were performed using the SYBYL 6.9 molecular modeling program package [12].

Gasteiger-Hückel [13] charges were assigned and then energy minimization of each molecule was performed using the conjugate gradient method and Tripos FF standard force field with a distance-dependent dielectric function. The minimization was terminated when the energy gradient convergence criterion of 0.001 kcal mol⁻¹·Å⁻¹ was reached.

The crystal structure of HIV-1 reverse transcriptase in complex with pyridazinone inhibitor (pdb id: 3DYA) [7] was downloaded from the protein data bank. GLIDE 4.0 [14] was used for molecular docking. The protein was prepared using protein preparation module applying the default parameters, a grid was generated around the non-nucleoside active site of the reverse transcriptase with receptor Van der Waals scaling for the non polar atoms as 0.9 [15]. The molecular docking of the 31 molecules into

Fig. 1 Common substructure used for alignment



the generated grid was performed by using the standard precision docking mode [15]. The crystal structure ligand was also docked and its RMSD was calculated to validate the docking process. The analysis of dock poses of all the molecules showed similar hydrogen bond interaction with the active site residues. The active conformation thus obtained was then aligned on docked poses of most active molecule in the series, molecule 30 using ALIGN DATABASE command in SYBYL 6.9 taking the substructure that is common to all (Fig. 1). The resulting alignment is shown in Fig. 2. This alignment process is a standard rigid RMSD overlay of selected common structural motive, where the docked poses of the most active molecule was used as a template on to which the dataset was aligned.

Standard Tripos force field was employed for the CoMFA and CoMSIA analysis. A 3D cubic lattice overlapping all entered molecules and extended by at least 4 Å in each direction with each lattice intersection of a regularly spaced grid of 2.0 Å was created. The steric and electrostatic parameters were calculated in case of the CoMFA fields, while hydrophobic, H-bond acceptor and H-bond donor parameters in addition to steric and electrostatic were calculated in case of the CoMSIA fields at each lattice. A sp^3 hybridized carbon atom was used as a probe atom to generate steric (Lennard-Jones potential) field energies and a charge of +1 to generate electrostatic (Coulombic potential) field energies. A distance dependent dielectric constant of 1.00 was used. The steric and electrostatic fields were truncated at +30.00 kcal mol⁻¹. The similarity indices descriptors were calculated using the same lattice box employed for CoMFA calculations, using sp^3 carbon as a probe atom with a +1 charge, +1

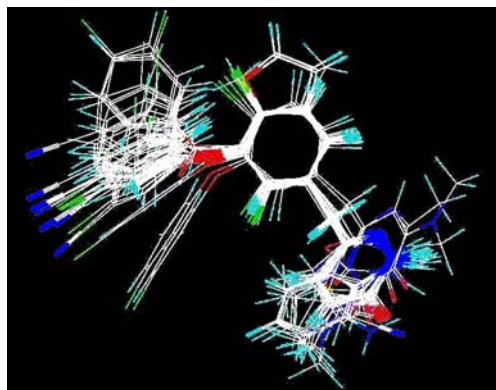


Fig. 2 Alignment of data set molecules based on common substructure using compound 30 as a template

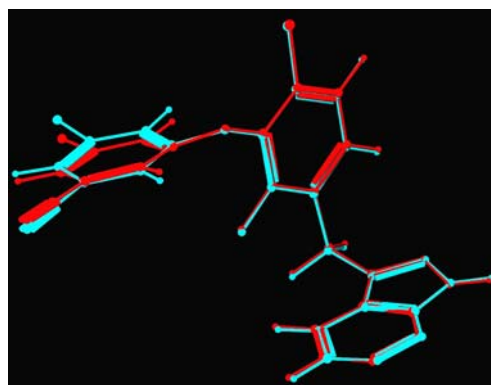


Fig. 3 Superimposition of crystal structure pose (cyan) on docked pose (red) of co-crystallized ligand. The RMS deviation is 0.151 Å

hydrophobicity and +1 H-bond donor and +1 H-bond acceptor properties.

A partial least squares regression was used to generate a linear relationship that correlates changes in the computed fields with changes in the corresponding experimental values of biological activity (pIC₅₀) for the data set of ligands. Biological activity values of ligands were used as dependent variables in a PLS statistical analysis. The column filtering value (s) was set to 2.0 kcal mol⁻¹ to improve the signal-to-noise ratio by omitting those lattice points whose energy variations were below this threshold. Cross-validations were performed by the leave-one-out (LOO) procedure to determine the optimum number of components (ONC) and the coefficient q^2 . The optimum number of components obtained is then used to derive the final QSAR model using all of the training set compounds with non-cross validation and to obtain the conventional correlation coefficient (r^2). To validate the CoMFA- and CoMSIA-derived models, the predictive ability for the test set of compounds (expressed as r^2_{pred}) was determined by using the following equation:

$$r^2_{pred} = (SD - PRESS) / SD$$

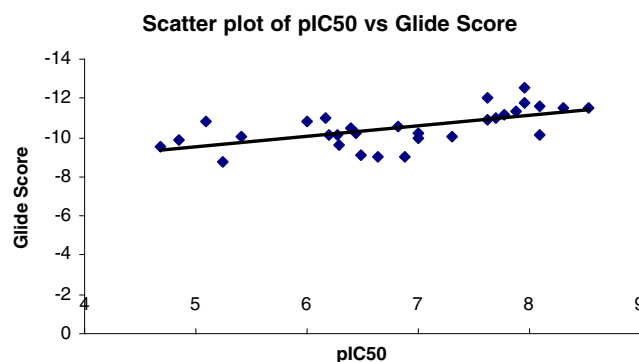


Fig. 4 Scatter plot of pIC₅₀ vs. glide score

Table 2 PLS result summary

Statistical parameters	CoMFA	CoMSIA 1	CoMSIA 2
q_{loo}^2	0.581	0.664	0.714
Number of molecules in training set	24	24	24
Number of molecules in test set	7	7	7
ONC	3	3	9
SEE	0.254	0.237	0.079
r^2	0.958	0.964	0.997
F_{ratio}	153.166	176.076	546.864
r_{pred}^2	0.5624	0.7317	0.7446
Fraction of field contributions			
Steric	0.479	0.142	0.172
Electrostatic	0.521	0.334	—
Hydrophobic	—	0.181	0.388
Acceptor	—	0.343	0.440

q_{loo}^2 = cross-validated correlation coefficient by leave one out method, r^2 = conventional correlation coefficient, ONC = optimum number of components, SEE = standard error of estimate, F = Fisher test value, r_{pred}^2 = cross-validated correlation coefficient on test set

SD is the sum of the squared deviations between the biological activities of the test set molecules and the mean activity of the training set compounds. PRESS is the sum of the squared deviation between the observed and the predicted activities of the test set compounds.

Since the statistical parameters were found to be the best for the model from the LOO method, it was employed for further predictions of the designed molecules. The designed molecules were also constructed, minimized and docked into the protein non-nucleoside site same as mentioned above.

Results and discussion

The best method of evaluating the accuracy of a docking procedure is to determine how closely the lowest energy pose (binding conformation) predicted by the object scoring function (Glide score), resembles an experimental binding mode as determined by X-ray crystallography. In the present study, standard precision glide docking procedure [15] was validated by removing compound 30 from the binding site and redocking it into the non-nucleoside

binding site of HIV-1 reverse transcriptase. We found a very good agreement between the localization of the inhibitor upon docking and from the crystal structure, *i.e.*, having similar hydrogen bonding interactions with Lys103, and it also showed good hydrophobic interaction with Tyr181, Tyr188, and Thr229. The root mean square deviations between the predicted conformation and the observed X-ray crystallographic conformation of compound 30 equaled 0.151 Å, a value that suggests the reliability of Glide docking in reproducing the experimentally observed binding mode for non-nucleoside HIV-1 reverse transcriptase inhibitor and the parameter set for the Glide docking is reasonable to reproduce the X-ray structure (Fig. 3). The correlation between dock score (glide score) and pIC_{50} gave a correlation coefficient value (r) of 0.595, which shows appreciable relation between biological activity and docking. Scatter plot of pIC_{50} and glide score is shown in Fig. 4.

The 3D QSAR – CoMFA and CoMSIA analysis were carried out using pyridazinones and triazolinones derivatives reported as potent non-nucleoside reverse transcriptase inhibitors by Sweeney et al. [5–7]. Molecules having

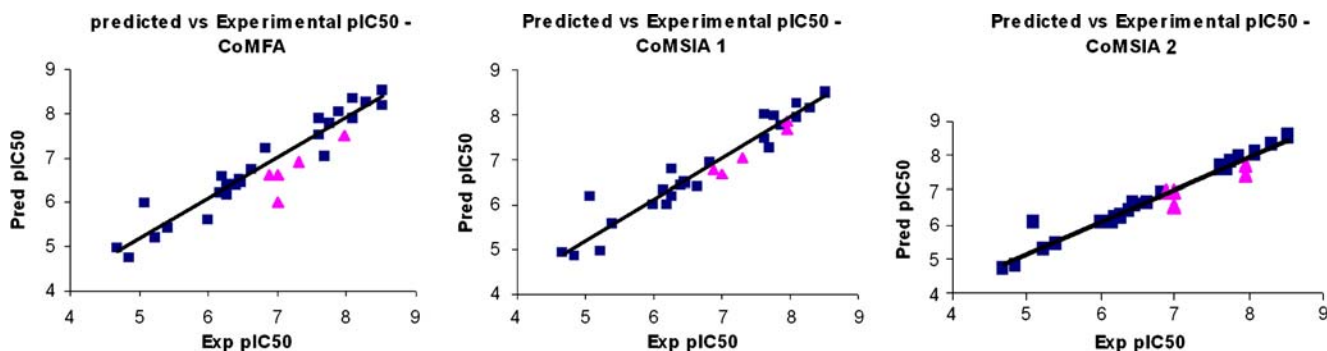


Fig. 5 Scatter plot of predicted vs. experimental pIC_{50} values (test set is represented as triangles)

Table 3 Experimental pIC₅₀, predicted pIC₅₀ and glide scores of the molecules

compound	IC ₅₀ in μM	pIC ₅₀	pred pIC ₅₀		pred pIC ₅₀	Glide Score
			CoMFA	CoMSIA 1		
1	21	4.678	4.982	4.946	4.719	-9.55
2	14	4.854	4.756	4.851	4.806	-9.84
3	0.64	6.194	6.579	5.997	6.178	-10.1
4 ^t	0.1	7	6.596	6.685	6.559	-10.23
5	0.52	6.284	6.166	6.178	6.168	-9.63
6	0.36	6.444	6.515	6.506	6.616	-10.2
7 ^t	0.1	7	6.004	6.661	6.966	-9.98
8	0.02	7.699	7.006	7.236	7.572	-10.97
9	0.23	6.6382	6.712	6.379	6.603	-9.02
10 ^t	0.13	6.886	6.595	6.801	6.93	-8.99
11	0.33	6.4815	6.415	6.457	6.516	-9.1
12 ^t	0.05	7.301	6.91	7.051	6.876	-10.08
13	0.15	6.824	7.191	6.94	6.863	-10.57
14	0.69	6.1612	6.206	6.325	6.075	-11.01
15	0.53	6.276	6.37	6.792	6.287	-10.14
16	5.8	5.237	5.208	4.971	5.288	-8.77
17	0.013	7.886	8.024	7.736	7.921	-11.3
18 ^t	0.011	7.959	7.517	7.671	7.444	-12.58
19	0.017	7.769	7.784	7.964	7.804	-11.14
20 ^t	0.011	7.959	7.52	7.873	7.762	-11.78
21	0.4	6.398	6.399	6.438	6.405	-10.49
22 ^t	8.2	5.086	5.972	6.181	6.055	-10.8
23	3.9	5.409	5.432	5.554	5.4	-10.03
24	1	6	5.62	5.989	6.066	-10.83
25	0.024	7.6197	7.5099	7.453	7.636	-10.95
26	0.024	7.6197	7.894	8.013	7.619	-12.06
27	0.008	8.0969	7.896	7.937	8.097	-10.12
28	0.008	8.0969	8.318	8.238	8.034	-11.6
29	0.005	8.301	8.248	8.138	8.291	-11.47
30	0.003	8.5228	8.53	8.482	8.53	-11.55
31	0.003	8.5228	8.187	8.493	8.547	-10.57

t = test set molecules, pIC₅₀ = -log IC₅₀

inhibitory activity against wild type HIV-1 reverse transcriptase enzyme with precise IC₅₀ values were selected. A total of 31 molecules were used for derivation of model, these were divided into a training set of 24 molecules and test set of seven, keeping in view that the activity range is with a minimum of 3 log unit differences in both the sets. The CoMFA and CoMSIA statistical analysis is summarized in Table 2. Statistical data shows q_{loo}^2 0.581 for CoMFA 0.664 for the CoMSIA models, r_{ncv}^2 of 0.958 and 0.964 for CoMFA and CoMSIA, respectively, which indicates a good internal predictive ability of the models. To test the predictive ability of the models, a test set of seven molecules excluded from the model derivation was used. The predictive correlation coefficient r_{pred}^2 of 0.5624

for CoMFA and 0.7317 for the CoMSIA models indicate good external predictive ability of the models. CoMSIA analysis was also performed by considering only steric, hydrophobic, and H-bond acceptor fields which gave q_{loo}^2 of 0.714 with ONC as 9. Non cross validate r^2 of 0.997 was obtained and showed r_{pred}^2 of 0.7446. The graph for the actual and predicted pIC₅₀ values for training set and test of CoMFA and CoMSIA studies shown in Fig. 5. The CoMSIA model showed better results than CoMFA model, this shows that the hydrophobic fields which were not included in the CoMFA model are important for explaining the potency of the molecules. This is also evident from the docking results. The predicted activity and glide scores of the molecules are provided in Table 3.

To visualize the information content of the derived 3D-QSAR model, CoMFA, and CoMSIA contour maps were generated. The contour plots are the representation of the lattice points and the difference in the molecular field values at lattice point is strongly connected with difference in the receptor binding affinity. Molecular fields define the favorable or unfavorable interaction energies of aligned

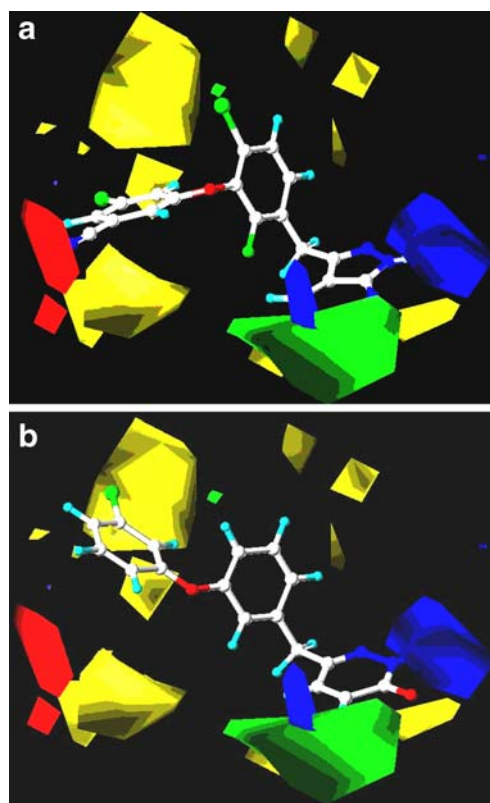


Fig. 6 CoMFA steric standard deviation (S.D.* coefficient) contour maps illustrating steric and electrostatic features in combination with compound (a) 30 and (b) 1. Green contours show favorable bulky group substitution at that point while yellow regions show unfavorable bulky group for activity. Red contours indicate negative charge favoring activity, whereas blue contours indicate positive charge favoring activity

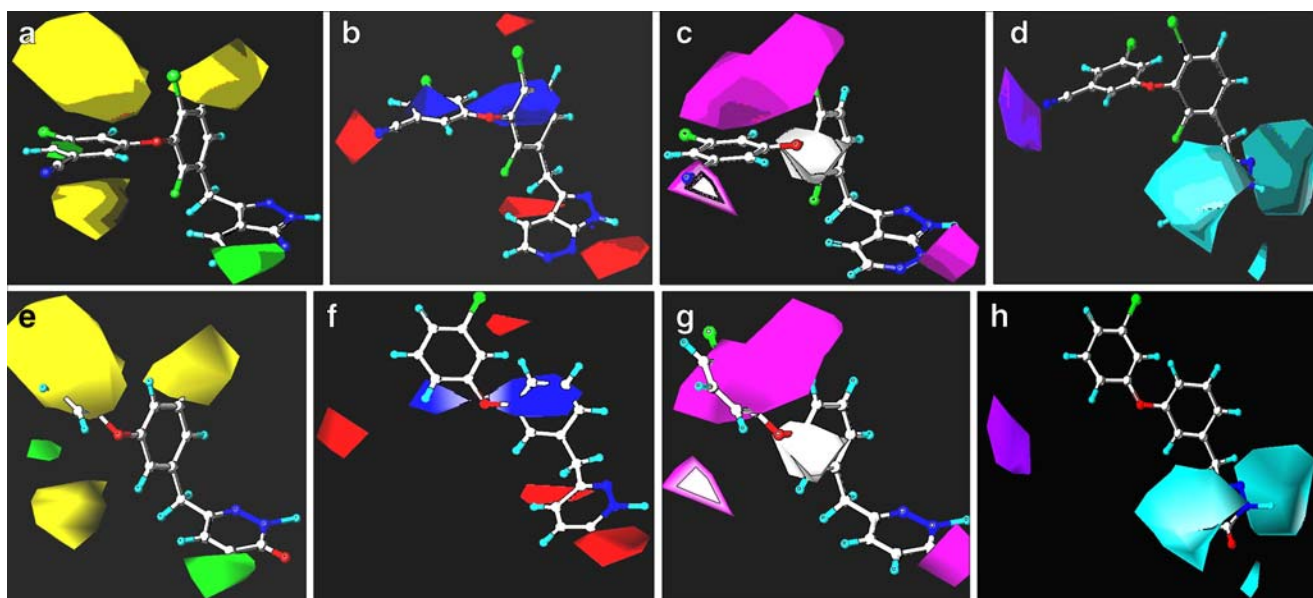


Fig. 7 CoMSIA S.D.* coefficient contour maps illustrating steric, electrostatic, acceptor and hydrophobic features in combination with compound **30**. **(a)** The green contour indicates a sterically favored region; yellow maps calls for a reduction of this potential to improve activity. **(b)** Blue indicates a positive charge preferred region to improve activity; Red indicates a negative charge preferred region to improve activity. **(c)** The magenta contour for hydrophobic favored region, white indicates the hydrophilic favored region **(d)**. The purple contour for H-bond acceptor group increases activity, cyan indicates the disfavored region. CoMSIA S.D.* coefficient contour maps

illustrating steric, electrostatic, acceptor and hydrophobic features in combination with compound **1**. **(e)** The green contour indicates a sterically favored region; yellow maps calls for a reduction of this potential to improve activity. **(f)** Blue indicates a positive charge preferred region to improve activity; Red indicates a negative charge preferred region to improve activity **(g)** The magenta contour for hydrophobic favored region, white indicates the hydrophilic favored region **(h)**. The purple contour for H-bond acceptor group increases activity, cyan indicates the disfavored region

molecules with a probe atom traversing across the lattice grid points surrounding the molecules. The 3D colored plots suggest the modification required to design new molecules.

The contour maps of CoMFA denote the region in the space where the aligned molecules would favorably or unfavorably interact with the receptor, while the CoMSIA contour maps denote those areas within the specified region where the presence of a group with a particular physico-chemical activity binds to the receptor. The CoMFA/CoMSIA results were graphically interpreted by field contribution maps using the ‘STDEV * COEFF’ field type.

Figure 6 (a, b) shows the contour maps derived from the CoMFA PLS model. The most potent analogue, compound **30**, was embedded in the map (a), while least active compound **1** was embedded in the map (b) to demonstrate its affinity for the steric and electrostatic regions of inhibitors. The areas of yellow indicate regions of steric hindrance to activity, while green areas indicate a steric contribution to potency. The blue regions indicate positive electrostatic charge potential associated with increased activity, while red region show negative charge potential.

All of the contours represented the default 80 and 20% level contributions for favored and disfavored regions, respectively. The pyrazole ring of **30** is in the sterically

favored green region for bulky groups and the chlorobenzonitrile is away from the yellow disfavored region for sterically bulky groups. The –CN group is oriented toward red region indicating favored negative electrostatic potentials, all these explain the high activity of the compound. The least active compound **1** has a pyridazin ring which is

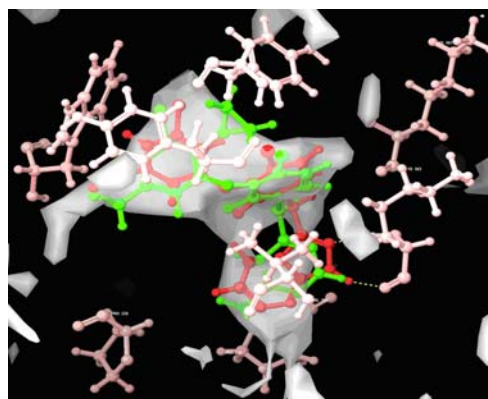


Fig. 8 Docked pose of molecule **30** (green) and **7a** (red) in the protein active site, showing the hydrophobic cavity and hydrogen bond interaction (yellow lines) with Lys103. The hydrophobic cavity crowded by the amino acids makes the site sterically disfavored for bulkier groups to bind

Fig. 9 Structural requirements for binding and inhibitory activity of pyridazinones and triazolinone

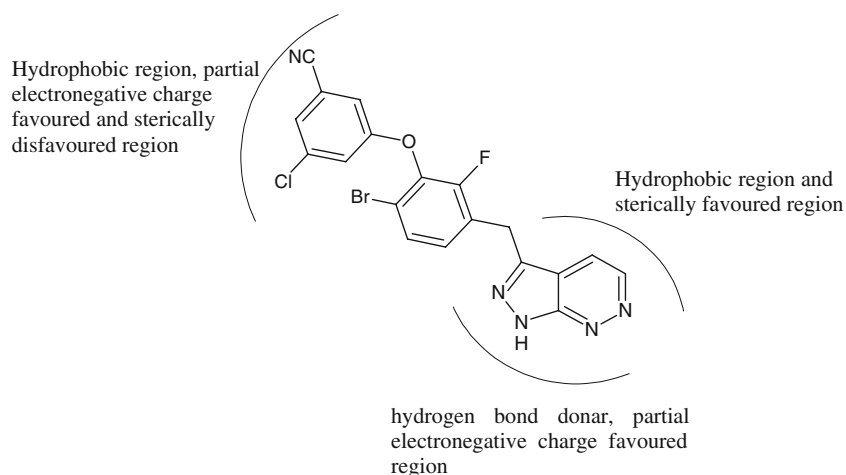


Fig. 10 Structure of newly designed molecules

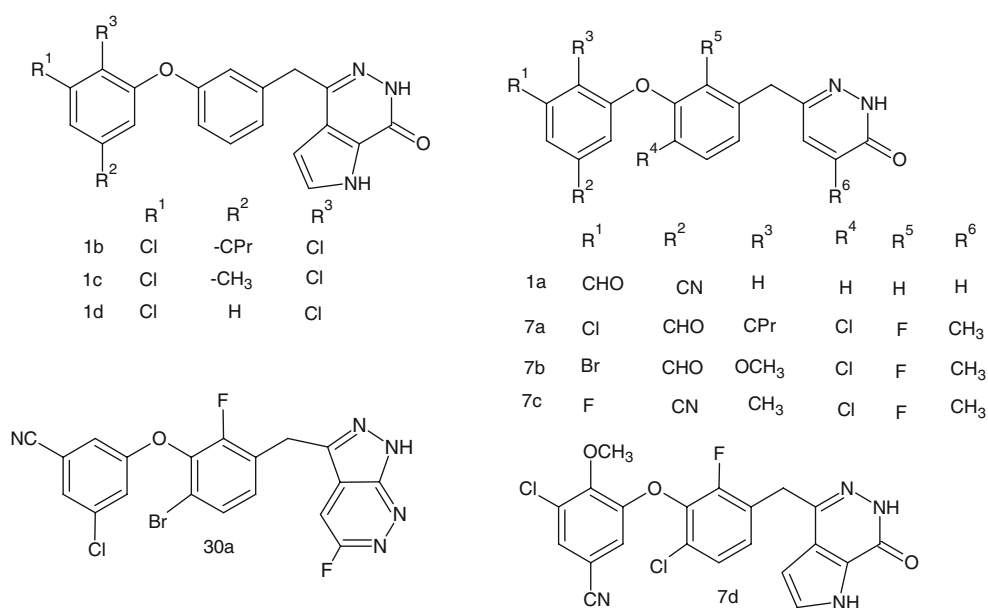


Table 4 Glide score and predicted activity of newly designed molecules

Compound	Pred pIC ₅₀	Pred pIC ₅₀	Pred pIC ₅₀	Glide score
	CoMFA	CoMSIA 1	CoMSIA 2	
1a	6.159	6.397	6.252	-9.89
1b	6.921	5.835	5.884	-10.26
1c	6.935	6.151	5.854	-10.01
1d	6.679	6.229	5.835	-9.74
7a	7.434	8.021	8.249	-10.18
7b	7.161	7.201	7.79	-10.44
7c	7.249	7.032	7.539	-10.11
7d	7.225	7.243	7.532	-10.5
30a	8.444	8.481	8.612	-11.49

away from the steric favored region. The presence of a bulkier group on pyridazin ring should increase the activity which is evident from compounds 6, 8, 9, 10, and 17 having a methyl substitution at the pyridazin ring. Chlorobenzene moiety is oriented toward the yellow region which is unfavorable for binding to receptor.

Figure 7 (a–h) shows the contour maps derived from the CoMSIA PLS model. The most potent analogue, compound 30, was embedded in the maps (a) to (d) while compound 1 was embedded in maps (e) to (h) to demonstrate its affinity for the steric, electrostatic, hydrophobic and H-bond acceptor regions of inhibitors.

The steric map is similar to the CoMFA steric map showing favored and disfavored regions. The difference in activity of compound 30 and 1 is shown by their orientation in the maps, chlorobenzene group of compound 1 is embedded inside the disfavored yellow region and the pyridazin ring is away from the green region, whereas in compound 30 the pyrazole ring is penetrating into the green region and the chlorobenzonitrile group is orienting away from the disfavored yellow region.

The electrostatic contour maps show a red region near the pyrazole ring in 30 and chlorobenzene ring in 1 indicating a negative electrostatic potential should increase the potency as seen in the case of 30. The blue regions near the central benzene ring indicates a region with positive electrostatic potentials.

The hydrophobic contours show a favored magenta region near the pyrazole and chlorobenzonitrile group and a disfavored white region near the central benzene ring for compound 30 and compound 1. The difference in activity of these two compounds can be explained by the overlap of the favored hydrophobic region with the disfavored steric region at the chlorobenzene ring. This is evident from the docking analysis that shows a hydrophobic pocket at the site created due to Tyr181, Tyr188, and Thr229 but the cavity is sterically crowded allowing less sterically bulky group to bind (Fig. 8). The favored hydrophobic region near the pyrazole ring is in accordance with the steric field which shows the favored region for sterically bulky groups. The acceptor contour maps show the favored region for hydrogen bond acceptor groups near the chlorobenzonitrile ring and a disfavored region for hydrogen bond acceptors near the pyrazole ring.

The detailed contour map analysis of both CoMFA and CoMSIA models empowered us to identify structural requirements for the observed inhibitory activity (Fig. 9). The molecules were modified to further improve the inhibition activity toward HIV-1 RT. Compound 1, 7, and 30 having least, medium and best activity respectively were chosen as a reference structure to design new molecules (Fig. 10), to obtain a greater number of new potent molecules. The newly designed molecules were docked

into the protein active site. Dock poses were used to predict the activity by applying the 3D-QSAR model. The new molecules showed better dock score and predicted activity (Table 4) than 1 and 7 but the modification done on 30 did not yield any promising ligands. Small hydrophobic groups (methyl, aldehydic, nitrile and cyclopropyl) substituted on the chlorobenzene ring increased the activity in the case of 1 and 7, due to major hydrophobic region in the active site of the receptor, large hydrophobic groups substituents will lead to steric clashes with the active site residues. Increasing the ring moiety (azole) at the pyridazin in 7d showed increased activity.

Conclusions

3D-QSARs are widely employed to develop new molecules that have an improved biological property. CoMFA and CoMSIA methodologies were used to build models for HIV-1 reverse transcriptase inhibitory activity of the pyridazinones and triazolinones derivatives. Based on the detailed contour map analysis, improvement in HIV-1 reverse transcriptase binding affinity can be achieved through conformationally restricted substitution at the chlorobenzene and chlorobenzonitrile ring, maintaining the hydrophobic character with less steric hindrance at these regions. The designed molecules based on these parameters showed better activity than the reference molecules, which indicates that the 3D-QSAR model generated has a good predictive ability and can be used to design new molecules with better activity. These molecules can be synthesized to generate a greater number of molecules with required pharmacokinetics for further clinical studies.

Acknowledgments We gratefully acknowledge support for this research from University Grants Commission, India, Department of Science and Technology, India and Department of chemistry, Nizam College, Hyderabad. We are greatly thankful to Dr. G. N. Shastry, Indian Institute of Chemical technology for Sybyl 6.9 software and his useful suggestions. We also acknowledge Schrödinger Inc. for GLIDE 4.0 software.

References

1. AIDS epidemic update, December 2006, UNAIDS/WHO, www.unaids.org
2. Zhou Z, Lin X, Madura JD (2006) HIV-1 RT nonnucleoside inhibitors and their interaction with RT for antiviral drug development. *Infect Disord: Drug Targets* 6:391–413
3. Xia Q, Radzio J, Erson K, Sluis C (2007) Probing nonnucleoside inhibitor-induced active-site distortion in HIV-1 reverse transcriptase by transient kinetic analyses. *Protein Sci* 16:1728–1737
4. Ren J, Stammers DK (2005) HIV reverse transcriptase structures: designing new inhibitors and understanding mechanisms of drug resistance. *Trends Pharmacol Sci* 26:4–7

5. Sweeney ZK, Acharya S, Adrew B, Dunn JP, Elworthy TR, Fretland J, Giannetti AM, Heilek G, Li Yu, Kaiser AC, Martin M, Saito DY, Smith M, Suh JM, Swallow S, Wu J, Hang JQ, Zhou AS, Klumpp K (2008) Discovery of triazolinone non-nucleoside inhibitors of HIV reverse transcriptase. *Bioorg Med Chem Lett* 18:4348–4351
6. Sweeney ZK, Dunn JP, Elworthy TR, Heilek G, Li Yu, Kaiser AC, Saito DY, Swallow S, Zhou AS, Klumpp K, Dunten P, Han X, Harris SF, Hirschfeld DR, Hogg JH, Walter H, Kertesz DJ, Kim W, Mirzadegan T, Roepel MG, Tania M, Silva PC, Tracy JL, Villasenor A, Vora H (2008) Discovery and optimization of pyridazinone non-nucleoside inhibitors of HIV-1 reverse transcriptase. *Bioorg Med Chem Lett* 18:4352–4354
7. Sweeney ZK, Harris SF, Arora N, Javanbakht H, Li Yu, Fretland J, Davidson JP, Billedeau JR, Gleason SK, Hirschfeld D, Joshun J, Smith K, Mirzadegan T, Roetz R, Smith M, Sperry S, Suh JM, Jeffery Wu, Tsing S, Villasenor AG, Paul A, Guoping Su, Heilek G, Hang JQ, Zhou AS, Jernelius JA, Zhang FJ, Klumpp K (2008) Design of Annulated Pyrazoles as inhibitors of HIV-1 reverse transcriptase. *J Med Chem* 51:7449–7458
8. Cramer RD 3rd, Patterson DE, Bunce JD (1988) Comparative molecular field analysis (CoMFA) 1. Effect of shape on binding of steroids to carrier proteins. *J Am Chem Soc* 110:5959–5967
9. Cramer RD 3rd, Patterson DE, Bunce JD (1988) Crossvalidation, bootstrapping, and partial least squares compared with multiple regression in conventional QSAR studies. *Quant Struct Act Relat* 7:18–25
10. Klebe G, Abraham U, Mietzner T (1994) Molecular similarity indices in a comparative analysis. *J Med Chem* 37:4130–4146
11. Wold S, Johansson A, Cochi M (1993) D-QSAR in drug design: theory, methods and application. In: Kubinyi H (ed) *PLS-Partial least squares projection to latent structures*. ESCOM, Lieden, pp 523–550
12. Sybyl version 6.9, Tripos Associates, St Louis (MO), 1999
13. Gasteiger J, Marsili M (1980) Iterative partial equalization of orbital electronegativity – a rapid access to atomic charges. *Tetrahedron* 36:3219–3228
14. Schrödinger LLC (2005) New York, NY, Glide, Version 4.0
15. Friesner RA, Banks JL, Murphy RB, Halgren TA, Klicic JJ, Mainz DT, Repasky MP, Knoll EH, Shelley M, Perry JK, Shaw DE, Francis P, Shenkin PS (2004) *J Med Chem* 47:1739–1749